Accepted by IEEE Transactions on Power Systems (doi: 10.1109/TPWRS.2018.2876429) in Oct. 2018

Voltage Stability Analysis of Power Systems with Induction Motors Based on Holomorphic Embedding

Rui Yao, *Member, IEEE,* Kai Sun, *Senior Member, IEEE,* Di Shi, *Senior Member, IEEE,* Xiaohu Zhang, *Member, IEEE*

***Abstract*—Load characteristics have substantial influence on the voltage stability of power systems. The self-restorative characteristic and stalling of induction motor loads can deteriorate the voltage stability, so it is necessary to develop accurate and efficient dynamic analysis methods for voltage stability analysis of systems with induction motor loads. In this paper, a set of methods based on holomorphic embedding is proposed, which is able to solve steady states and dynamics of a power system with induction motors. The paper is the first work that applies holomorphic embedding to dynamic problems of power systems. The test cases on the IEEE 14-bus system, the NPCC 140-bus system and the Polish 2383-bus system verify both accuracy and efficiency of the proposed methods.**

***Index Terms*—Voltage stability, load model, induction motor, stability analysis, approximation, dynamic simulation, analytical method, holomorphic embedding, quasi-steady-state.**

I. Introduction

INDUCTION motor loads have significant influence on voltage stability of power systems [1]–[3]. The self-restorative characteristic of induction motors contributes to voltage instability. Moreover, the low voltage caused by insufficient voltage support or faults can cause motors to stall. The stalling motors cause delayed voltage recovery and thus exacerbate voltage instability [4]. The voltage stability analysis (VSA) with induction motor loads has been studied or discussed in some literature over the past years. Strictly speaking, the VSA with induction motors is a dynamic problem [1], [5]–[7], but the traditional dynamic simulation methods based on numerical integration are computationally expensive [8], [9]. For long-term VSA with slow load growth, the generator and motor dynamics are much faster than the load increase, and thus a quasi-steady state (QSS) method can be utilized. The QSS method degenerates differential equations of the studied system to algebraic equations, and replaces the time-domain solutions of differential-algebraic equations by the trace of algebraic equation solutions [10]. In either the dynamic simulation or the QSS method, solving nonlinear algebraic equations is necessary. However, in traditional VSA methods, solving the algebraic equations may suffer from numerical problems, especially when the system is close to singularity. In summary, the conventional VSA methods have two major difficulties: 1) the inefficiency of dynamic simulation based on numerical integration technique; 2) the difficulty of numerical convergence when solving nonlinear algebraic equations.

In recent years, the holomorphic embedding (HE) method has been utilized to solve algebraic equations of power systems and achieved considerable success in improving the convergence and computational efficiency [11]–[17]. The HE method represents the solution of the equations as a power series of an embedding variable in the complex domain despite the fact that a practical solution always has the embedding variable take a real value. At the original point of the power series, the solution is already known or easily acquired. Thus, the computation of HE is to derive the coefficients in the power series. The Padé approximation can also be used to further increase the convergence range of the series [18]. Moreover, the multi-stage HE method proposed in [19] for static VSA can improve precision and effectively reduce the number of terms in Padé approximants.

As commented in [12] and [15], the HE is a high-order analytic continuation method and thus has a much larger effective range than the traditional homotopy method which uses a limited order for continuation. Therefore, as a very promising methodology for static VSA, HE can be further extended to solve the power flow equations with more complex loads like induction motor models. Moreover, considering the essence of the popular numerical integration methods for dynamic simulation (e.g. the Euler method and Runge-Kutta method), they can only limit the error to a relatively low order, and thus the time step is constrained to a very small number. Analogously, the idea of HE can also be utilized in dynamic simulation to achieve much larger time steps of computation, thus significantly reducing the number of steps and improving the speed of simulation.

This paper studies the voltage stability analysis with the presence of induction motor loads by using HE. The major contributions of this paper are:

1) The HE formulations of induction motor models are proposed, which enriches the capability of HE methodology in power system analysis.

This work was supported in part by the ERC Program of the NSF and DOE under NSF grant EEC-1041877, in part by NSF grant ECCS-1610025 and in part by the SGCC Science and Technology Program under grant 5455HJ160007. (*Corresponding author: Kai Sun*)

R. Yao is with the Argonne National Laboratory, Lemont, IL 60439, USA and University of Tennessee, Knoxville, TN 37996, USA (email: yaorui.thu@gmail.com).

K. Sun is with the Department of EECS, the University of Tennessee, Knoxville, TN 37996, USA (email: kaisun@utk.edu).

D. Shi and X. Zhang are with GEIRI North America, San Jose, CA 95134, USA.

2) The HE formulations utilize grid-load interface, with which the computation of the grid and the loads is decomposed and the computation tasks on different loads can be parallelized, so the computation efficiency is enhanced.

3) The dynamic simulation for VSA based on HE is realized. This is the first research work using HE for dynamic analysis in power systems. With HE, the time step in simulation is much larger than that in the traditional methods, and the computation speed is significantly improved.

The rest of the paper is organized as follows. The HE formulations and algorithms for power flow, static VSA and the dynamic simulation for VSA with induction motors are proposed in Section II. The multi-stage VSA based on QSS and dynamic simulation with HE are proposed in Section III. The test cases on the IEEE 14-bus system, the NPCC 140-bus system and the Polish 2383-bus system are in Section IV. Section V is the conclusion.

II. Holomorphic embedding formulations

A. HE-I: solving power flow from trivial germ solution

From the grid side, the power flow equation on each bus is

$$S_i^* W_i^* - \sum_l Y_{il}^{tr} V_l - Y_i^{sh} V_i - I_{Li} = 0, \tag{1}$$

where "*" means conjugation, V_i is the voltage phasor on bus i, whose reciprocal is W_i. For PQ buses, $S_i = P_i + jQ_i$ is given. For PV buses, P_i is given, and the voltage should satisfy magnitude constraint $V_i V_i^* = |V_i^{sp}|^2$. The V_i^{sp} means a specified voltage phasor. For PV buses, only its magnitude $|V_i^{sp}|$ is needed, so the angle of phasor V_i^{sp} can be simply set as 0, and the magnitude is set as $|V_i^{sp}|$. For the swing bus, the complete phasor V_i^{sp} is known. Y_{il}^{tr} is the serial branch admittance between buses i and l, and Y_i^{sh} is the shunt admittance on bus i. I_{Li} is the total load current (except const-PQ and const-impedance loads that have been included in S_i and Y_i^{sh}) on bus i. The HE formulation for solving power flow is constructed as follows:

$$S_i(\alpha)^* W_i^*(\alpha) - \sum_l Y_{il}^{tr} V_l(\alpha) - \alpha Y_i^{sh} V_i(\alpha) - I_{Li}(\alpha) = 0, \tag{2}$$

where the embedding variable $\alpha \in \mathbb{C}$. For PQ buses, $S_i(\alpha) = \alpha(P_i + jQ_i)$ is known. For PV buses $S_i(\alpha) = \alpha P_i + jQ_i(\alpha)$ and reactive power $Q_i(\alpha)$ needs to be calculated. And the HE formulations of the voltages on PV and slack buses are

$$\begin{aligned} &V_i(\alpha) V_i^*(\alpha) - 1 - \alpha(|V_i^{sp}|^2 - 1) = 0, i \in S_{PV} \\ &V_i(\alpha) - 1 - \alpha(V_i^{sp} - 1) = 0, i \in S_{SL}, \end{aligned} \tag{3}$$

where S_{PV} and S_{SL} represent the sets of PV and slack buses, respectively. The term "trivial germ solution" is the state $V_i[0] = 1$, $Q_i[0] = 0$ (for PV buses) and $I_{Li}[0] = 0$. The trivial germ solution satisfies (2) and (3) when $\alpha = 0$. The variables in HE are represented as power series of α, such as

$$V_i(\alpha) = V_i[0] + V_i[1]\alpha + V_i[2]\alpha^2 + V_i[3]\alpha^3 + \cdots. \tag{4}$$

In this paper, each coefficient of the power series is denoted by the variable name followed by a square-bracketed index, e.g. $V_i[k]$ for $V_i(\alpha)$. HE solves the coefficients like $V_i[n]$. Similar to [13], $V_i[n]$ and $Q_i[n]$ are obtained by solving (5):

$$\begin{aligned} &\begin{bmatrix} -B_{11} & G_{11} & \cdots & -B_{1i} & 0 & \cdots & -B_{1N} & G_{1N} \\ G_{11} & B_{11} & \cdots & G_{1i} & 0 & \cdots & G_{1N} & B_{1N} \\ \vdots & \vdots & \vdots & \vdots & \vdots & \vdots & \vdots & \vdots \\ -B_{i1} & G_{i1} & \cdots & -B_{ii} & 0 & \cdots & -B_{iN} & G_{iN} \\ G_{i1} & B_{i1} & \cdots & G_{ii} & 1 & \cdots & G_{iN} & B_{iN} \\ \vdots & \vdots & \vdots & \vdots & \vdots & \vdots & \vdots & \vdots \\ -B_{N1} & G_{N1} & \cdots & -B_{Ni} & 0 & \cdots & -B_{NN} & G_{NN} \\ G_{N1} & B_{N1} & \cdots & G_{Ni} & 0 & \cdots & G_{NN} & B_{NN} \end{bmatrix} \begin{bmatrix} D_1[n] \\ C_1[n] \\ \vdots \\ D_i[n] \\ Q_i[n] \\ \vdots \\ D_N[n] \\ C_N[n] \end{bmatrix} \\ &= \begin{bmatrix} \Re(\Gamma_1[n]) \\ \Im(\Gamma_1[n]) \\ \vdots \\ \Re(\Gamma_i[n]) \\ \Im(\Gamma_i[n]) \\ \vdots \\ \Re(\Gamma_N[n]) \\ \Im(\Gamma_N[n]) \end{bmatrix} - \sum_{j \in S_{PV} \bigcup S_{SL}} \begin{bmatrix} G_{1j} \\ B_{1j} \\ \vdots \\ G_{ij} \\ B_{ij} \\ \vdots \\ G_{Nj} \\ B_{Nj} \end{bmatrix} C_j[n] - \sum_{j \in S_{SL}} \begin{bmatrix} -B_{1j} \\ G_{1j} \\ \vdots \\ -B_{ij} \\ G_{ij} \\ \vdots \\ -B_{Nj} \\ G_{Nj} \end{bmatrix} D_j[n], \end{aligned} \tag{5}$$

where G_{il} and B_{il} are real and imaginary parts of the admittance Y_{il}^{tr}. $C_i[n]$ and $D_i[n]$ are real and imaginary parts of $V_i[n]$. $\Re(\cdot)$ and $\Im(\cdot)$ are real and imaginary operators. In (5), for PQ buses,

$$\Gamma_i[n] = S_i^* W_i^*[n-1] - Y_i^{sh} V_i[n-1] - I_{Li}[n], \tag{6}$$

and for PV buses,

$$\Gamma_i[n] = P_i W_i^*[n-1] - j \sum_{k=0}^{n-1} Q_i[k] W_i^*[n-k] - Y_i^{sh} V_i[n-1] - I_{Li}[n]. \tag{7}$$

From (3) the $C[n]$ terms on the right-hand side of (5) are

$$C_i[n] = \frac{1}{2C_i[0]} \left(\delta_{n,1}(|V_i^{sp}|^2 - 1) - \sum_{k=1}^{n-1} V_i[k] V_i^*[n-k] \right), \tag{8}$$

where $\delta_{n,1}$ is 1 for $n = 1$ and 0 for $n \neq 1$. To solve (5), the load current $I_{Li}[n]$ should be determined first. $I_{Li}[n]$ can be viewed as a load-grid interface, which decomposes the computation of the grid and loads. Here we only discuss $I_{Li}[n]$ as the current of induction motors. If there are multiple induction motors (labeled as m) on bus i, then

$$I_{Li}[n] = \sum_m I_{Lim}[n]. \tag{9}$$

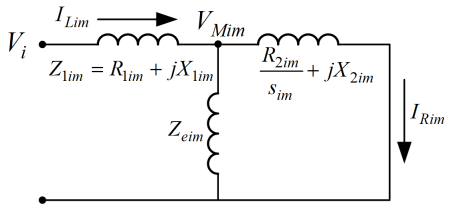

Fig. 1. Equivalent circuit of induction motor.

Next, the HE formulation of an induction motor will be established. As a general guideline, the HE formulation should satisfy the following requirements.

1) The correctness of the mathematical model. At $\alpha = 1$, the HE formulation must be equivalent to the original mathematical model of the studied element or system.

2) The germ solution should be easy to obtain. At $\alpha = 0$, the solution of the HE formulation is either trivial or known.

Take the most commonly used model of induction motors for analysis, whose equivalent circuit is shown in Fig. 1. The circuit has an internal node whose voltage is denoted as $V_{Mim}(\alpha)$. Following the above-mentioned rules, the construction of the trivial germ solution should satisfy: 1) the voltages on all buses are identical. 2) the current on each branch is 0. Thus consequently, the admittance of every shunt branch should be 0. So in the HE formulation of induction motors, the impedance of the excitation branch is constructed as Z_{eim}/α to make 0 admittance. While for the rotor side, the manipulation can be achieved by modifying the mechanical torque as $\alpha T_{im}(s_{im})$. When $\alpha = 0$, the zero mechanical torque will guarantee $I_{Rim} = 0$. The following equations are listed for HE:

$$\begin{aligned} &V_{Mim}(\alpha) = V_i(\alpha) - I_{Lim}(\alpha)Z_{1im} \\ &I_{Lim}(\alpha) = I_{Rim}(\alpha) + \frac{\alpha V_{Mim}(\alpha)}{Z_{eim}} \\ &I_{Rim}(\alpha)I^*_{Rim}(\alpha) = \frac{\alpha T_{im}(s_{im}(\alpha))s_{im}(\alpha)}{R_{2im}} \\ &I_{Rim}(\alpha)\left(R_{2im} + jX_{2im}s_{im}(\alpha)\right) = V_{Mim}(\alpha)s_{im}(\alpha), \end{aligned} \tag{10}$$

where the mechanical torque T_{im} depends on the slip s_{im}, and usually it is assumed as a quadratic function of s_{im} [20]

$$T_{im}(s_{im}) = T_{0im} + T_{1im}s_{im} + T_{2im}s^2_{im}. \tag{11}$$

The germ solution of the embedding form (10) is $V_{Mim}[0] = 1$, $I_{Lim}[0] = 0$, $I_{Rim}[0] = 0$, $s_{im}[0] = 0$. From (10), the equations of the coefficients (12)-(15) are obtained ((14) and (15) are at the bottom of the page):

$$I_{Lim}[n] = I_{Rim}[n] + \frac{V_{Mim}[n-1]}{Z_{eim}}, \tag{12}$$

$$V_{Mim}[n] = V_i[n] - I_{Lim}[n]Z_{1im}, \tag{13}$$

When $n = 1$, (14) and (15) become:

$$I_{Rim}[1]I^*_{Rim}[1] = \frac{T_{0im}s_{im}[1]}{R_{2im}}, \tag{16}$$

$$I_{Rim}[1]R_{2im} = V_{Mim}[0]s_{im}[1]. \tag{17}$$

From (16) and (17),

$$I_{Rim}[1] = T_{0im}, s_{im}[1] = T_{0im}R_{2im}. \tag{18}$$

When $n > 1$, note that $I_{Rim}[0] = 0$, $s_{im}[0] = 0$, (14)-(15) become linear equations of $I_{Rim}[n]$ and $s_{im}[n]$. Therefore, $I_{Rim}[n]$ and $s_{im}[n]$ can be solved from (14)-(15), and $I_{Lim}[n]$ is obtained from (12). The load current term $I_{Lim}[n]$ is put into (5) and the states in the grid $V_i[n]$, $W_i[n]$, $Q_i[n]$ are solved. Finally, with $V_i[n]$ and $I_{Lim}[n]$, $V_{Mim}[n]$ is obtained from (13). Such a procedure is clearly structured as the load-grid two-stage computation. Also, since solving (12)-(15) does not involve the variables other than the studied induction motor, here the states of all induction motors can be calculated in parallel. Moreover, it is proven that HE-I generally guarantees convergence to the low-slip stable solution (see Appendix A).

B. HE-II: continuation from non-trivial germ

The HE-I is for the computation of a single power flow state, and its germ solution usually does not correspond to a real state. In VSA, it is desirable to study the trace of system states when the system configuration changes, e.g. load increases in a direction. Deriving and solving such a problem (denoted as HE-II) is similar, i.e. describing the variables as a power series of α and then solve the coefficients of the series. Denoting the embedding variable α as the loading factor, the HE formulation for bus i is

$$(P_i(\alpha) - jQ_i(\alpha))W^*_i(\alpha) - \sum_l Y_{il}V_l(\alpha) - I_{Li}(\alpha) = 0. \tag{19}$$

For PQ buses, the $P_i(\alpha)$ and $Q_i(\alpha)$ are known, while for PV buses, only $P_i(\alpha)$ is known and $Q_i(\alpha)$ is to be calculated. The voltage equations for PV and slack buses are:

$$\begin{aligned} &V_i(\alpha)V^*_i(\alpha) = |V^{sp}_i|^2, i \in S_{PV} \\ &V_i(\alpha) = V^{sp}_i, i \in S_{SL}. \end{aligned} \tag{20}$$

From (19)-(20) the coefficients of the HE satisfy

$$\sum_{k=0}^{n}\left(P_i[k] - jQ_i[k]\right)W^*_i[n-k] - \sum_l Y_{il}V_l[n] - I_{Li}[n] = 0, \tag{21}$$

$$\sum_{k=0}^{n} V_i[k]V^*_i[n-k] = \begin{cases} |V^{sp}_i|^2, & n = 0 \\ 0, & n > 0 \end{cases}. \tag{22}$$

For the induction motor loads, the equations are:

$$\begin{aligned} &V_{Mim}(\alpha) = V_i(\alpha) - I_{Lim}(\alpha)Z_{1im} \\ &I_{Lim}(\alpha) = I_{Rim}(\alpha) + \frac{V_{Mim}(\alpha)}{Z_{eim}} \\ &\Re\{V_{Mim}(\alpha)I^*_{Rim}(\alpha)\} = (r_{0im} + r_{1im}\alpha)T_{im}(s_{im}(\alpha)) \\ &I_{Rim}(\alpha)\left(R_{2im} + jX_{2im}s_{im}(\alpha)\right) = V_{Mim}(\alpha)s_{im}(\alpha), \end{aligned} \tag{23}$$

where r_{0im} is the base mechanical torque level, and r_{1im} represents the growth direction of mechanical torque.

$$\begin{aligned} &\sum_{k=0}^{n+1} I_{Rim}[k]I^*_{Rim}[n+1-k] \\ &\quad = \frac{1}{R_{2im}}\left(T_{0im}s_{im}[n] + T_{1im}\sum_{k=0}^{n} s_{im}[k]s_{im}[n-k] + T_{2im}\sum_{k=0}^{n}\sum_{l=0}^{n-k} s_{im}[k]s_{im}[l]s_{im}[n-k-l]\right), \end{aligned} \tag{14}$$

$$I_{Rim}[n]R_{2im} + jX_{2im}\sum_{k=0}^{n} I_{Rim}[k]s_{im}[n-k] = \sum_{k=0}^{n} V_{Mim}[k]s_{im}[n-k]. \tag{15}$$

It should be noted that although the formulations of HE-I and HE-II look similar, the underlying studied problem and the physical meaning are different. For HE-I, the purpose is to obtain a single steady-state power flow solution corresponding to $\alpha = 1$. In HE-I, α is only an embedding variable connecting between the trivial germ solution ($\alpha = 0$) and the desired solution ($\alpha = 1$), and it does not have a physical meaning. While the purpose of HE-II is to study the trace of system state when the load increases. In HE-II, α represents the loading factor. Any $\alpha \in \mathbb{R}$ can represent a physically existing state of the system. So in (23) the induction motor should keep the excitation impedance as Z_{eim} rather than Z_{eim}/α in (10). In steady-state VSA, it is usually assumed that the load grows linearly with the loading factor, so in (19), the active and reactive power are expressed as $P_i(\alpha) = P_{0i} + \alpha P_{1i}$ and $Q_i(\alpha) = Q_{0i} + \alpha Q_{1i}$, respectively. Similarly in (23), the term $(r_{0im} + r_{1im}\alpha)T_{im}(s_{im}(\alpha))$ represents the linear growth of mechanical torque with loading factor α. To solve HE-II, it is assumed that the germ solution (which is a steady-state physical solution) is known. The germ solution can be given by HE-I/II or other methods for solving power flows. Generally, given the analytic algebraic equations, a proper HE formulation can be established and the problem can be solved. So the application can also be further extended to include generation control [21], outage analysis [22], [23], etc.

From (20)-(22), and renumbering the PQ buses before the PV buses, the HE coefficients can be derived by solving the following equations:

$$
\begin{bmatrix}
-G & B & \mathcal{D}(P[0]) & -\mathcal{D}(Q[0]) & 0 \\
-B & -G & -\mathcal{D}(Q[0]) & -\mathcal{D}(P[0]) & -\mathcal{D}(F_{PV}[0]) \\
 & & & & 0 \\
 & & & & -\mathcal{D}(E_{PV}[0]) \\
0 \;\; \mathcal{D}(C_{PV}[0]) & 0 \;\; \mathcal{D}(D_{PV}[0]) & 0 & 0 & 0 \\
\mathcal{D}(E[0]) & -\mathcal{D}(F[0]) & \mathcal{D}(C[0]) & -\mathcal{D}(D[0]) & 0 \\
\mathcal{D}(F[0]) & \mathcal{D}(E[0]) & \mathcal{D}(D[0]) & \mathcal{D}(C[0]) & 0
\end{bmatrix}
\begin{bmatrix} C[n] \\ D[n] \\ E[n] \\ F[n] \\ Q_{PV}[n] \end{bmatrix}
$$

$$
= \begin{bmatrix}
\Re\left(-\sum_{k=1}^{n} P_{PQ}[k] \circ W^*_{PQ}[n-k] + j\sum_{k=1}^{n} Q_{PQ}[k] \circ W^*_{PQ}[n-k] + I_{LPQ}[n]\right) \\
\Re\left(-\sum_{k=1}^{n} P_{PV}[k] \circ W^*_{PV}[n-k] + j\sum_{k=1}^{n} Q_{PV}[k] \circ W^*_{PV}[n-k] + I_{LPV}[n]\right) \\
\Im\left(-\sum_{k=1}^{n} P_{PQ}[k] \circ W^*_{PQ}[n-k] + j\sum_{k=1}^{n} Q_{PQ}[k] \circ W^*_{PQ}[n-k] + I_{LPQ}[n]\right) \\
\Im\left(-\sum_{k=1}^{n} P_{PV}[k] \circ W^*_{PV}[n-k] + j\sum_{k=1}^{n} Q_{PV}[k] \circ W^*_{PV}[n-k] + I_{LPV}[n]\right) \\
-\frac{1}{2}\sum_{k=1}^{n-1} V_{PV}[k] \circ V^*_{PV}[n-k] \\
\Re\left(-\sum_{k=1}^{n-1} W[k] \circ V[n-k]\right) \\
\Im\left(-\sum_{k=1}^{n-1} W[k] \circ V[n-k]\right)
\end{bmatrix}, \tag{24}
$$

where E_i and F_i are real and imaginary parts of W_i, $\mathcal{D}(\cdot)$ means diagonal matrix, "$\circ$" means element-wise product.

Similar to HE-I, eq. (24) contains terms of induction motor currents $I_{LPQ}[n]$ and $I_{LPV}[n]$ (denoting $I_{Lim}[n]$ on PQ and PV buses, respectively). From (23), the HE formulation of each induction motor has the equations (25) (next page). The terms a_{im}, b_{im}, and c_{im} in (25) are listed separately as follows:

$$a_{im} = -I_{Rim\mathrm{Im}}[0]X_{2im} - C_i[0] + I_{Lim\mathrm{Re}}[0]R_{1im} - I_{Lim\mathrm{Im}}[n]X_{1im} \tag{26}$$

$$b_{im} = I_{Rim\mathrm{Re}}[0]X_{2im} - D_i[0] + I_{Lim\mathrm{Re}}[0]X_{1im} + I_{Lim\mathrm{Im}}[n]R_{1im} \tag{27}$$

$$c_{im} = -r_{0im}\left(T_{1im} + 2T_{2im}s_{im}[0]\right). \tag{28}$$

Eq. (25) has 7 unknowns and 5 equations. Eliminating $I_{Rim\mathrm{Re}}[n]$, $I_{Rim\mathrm{Im}}[n]$ and $s_{im}[n]$, the load currents $I_{Lim\mathrm{Re}}[n]$, $I_{Lim\mathrm{Im}}[n]$ change linearly with $C_i[n]$ and $D_i[n]$:

$$\begin{bmatrix} I_{Lim\mathrm{Re}}[n] \\ I_{Lim\mathrm{Im}}[n] \end{bmatrix} = A_{im}\begin{bmatrix} C_i[n] \\ D_i[n] \end{bmatrix} + B_{im}. \tag{29}$$

Aggregating all the currents of motor loads on each bus

$$\begin{bmatrix} I_{Li\mathrm{Re}}[n] \\ I_{Li\mathrm{Im}}[n] \end{bmatrix} = \left(\sum_m A_{im}\right)\begin{bmatrix} C_i[n] \\ D_i[n] \end{bmatrix} + \sum_m B_{im}, \tag{30}$$

and substituting (30) into (24) and canceling I_L terms, the grid terms $C[n]$, $D[n]$, $E[n]$, $F[n]$ and $Q_{PV}[n]$ are solved. Placing $C[n]$, $D[n]$ back to (25) will solve the states of induction motors $I_{Rim\mathrm{Re}}[n]$, $I_{Rim\mathrm{Im}}[n]$, $I_{Lim\mathrm{Re}}[n]$, $I_{Lim\mathrm{Im}}[n]$ and $s_{im}[n]$.

As for the computational complexity of HE-II, the major computation burden is on solving the linear equations in (24) and (25). Since the matrices are constant, the factorization of matrices is needed only once and the computation can be significantly accelerated.

C. HE-III: solving dynamics of induction motors

HE-II is based on the QSS assumption without dynamic modeling. However, when analyzing motor stalling, dynamic modeling and simulation in time domain is necessary. In the formulation of HE-II, with a common assumption in steady-state VSA that the loading factor increases linearly with time, the loading factor α also implicitly represents the time elapse. If t is explicitly used instead of α as the embedding variable, the solution naturally gives the evolution of states in time domain. In this regard, the HE-III formulation is proposed, which applies the holomorphic embedding into dynamic simulation.

In VSA, assume the system does not have any angle stability problem, so the dynamic models of synchronous generators are not considered, and the generator buses are still modeled as constant-voltage sources connected to PV or slack buses. Therefore, in HE-III, the power flow equations of the system except for induction motors are the same as those in HE-II. In long-term VSA, the electro-magnetic transients of motors can also be neglected, and differential equations only include rotor acceleration equations:

$$2H_{im}\frac{\mathrm{d}s_{im}}{\mathrm{d}t} = (r_{0im} + r_{1im}t)T_{im}(s_{im}) - \Re\{V_{Mim}I^*_{Rim}\}. \tag{31}$$

In HE-III, the embedding variable becomes time t, and the solution represents the evolution of states in time domain. Take (31) as an example. Assume the slip $s_{im}(t)$ as

$$s_{im}(t) = \sum_{k=0}^{\infty} s_{im}[k]t^k, \tag{32}$$

then the derivative of s_{im} with respect to t is

$$\frac{\mathrm{d}s_{im}}{\mathrm{d}t} = \sum_{k=1}^{\infty} k s_{im}[k]t^{k-1}. \tag{33}$$

$$
\left[\begin{array}{c|c|c|c|c|c|c}
R_{2im} & -X_{2im}s_{im}[0] & R_{1im}s_{im}[0] & -X_{1im}s_{im}[0] & a_{im} & -s_{im}[0] & 0 \\
\hline
X_{2im}s_{im}[0] & R_{2im} & X_{1im}s_{im}[0] & R_{1im}s_{im}[0] & b_{im} & 0 & -s_{im}[0] \\
\hline
\Re\{V_{Mim}[0]\} & \Im\{V_{Mim}[0]\} & 0 & 0 & c_{im} & 0 & 0 \\
\hline
-1 & 0 & 1+\Re(Z_{1im}/Z_{eim}) & -\Im(Z_{1im}/Z_{eim}) & 0 & -\Re(1/Z_{eim}) & \Im(1/Z_{eim}) \\
\hline
0 & -1 & \Im(Z_{1im}/Z_{eim}) & 1+\Re(Z_{1im}/Z_{eim}) & 0 & -\Im(1/Z_{eim}) & -\Re(1/Z_{eim})
\end{array}\right]
\left[\begin{array}{c} I_{Rim\mathrm{Re}}[n] \\ I_{Rim\mathrm{Im}}[n] \\ I_{Lim\mathrm{Re}}[n] \\ I_{Lim\mathrm{Im}}[n] \\ s_{im}[n] \\ C_i[n] \\ D_i[n] \end{array}\right]
$$

$$
= \left[\begin{array}{c}
\Re\left(\sum_{k=1}^{n-1} V_{Mim}[k]s_{im}[n-k] - jX_{2im}\sum_{k=1}^{n-1} I_{Rim}[k]s_{im}[n-k]\right) \\
\hline
\Im\left(\sum_{k=1}^{n-1} V_{Mim}[k]s_{im}[n-k] - jX_{2im}\sum_{k=1}^{n-1} I_{Rim}[k]s_{im}[n-k]\right) \\
\hline
-\Re\{\sum_{k=1}^{n} V_{Mim}[k]I^*_{Rim}[n-k]\} + r_{0im}\left(T_{2im}\sum_{k=1}^{n-1} s_{im}[k]s_{im}[n-k]\right) \\
+r_{1im}\left(T_{0im}\delta(n,1) + T_{1im}s_{im}[n-1] + T_{2im}\sum_{k=0}^{n-1} s_{im}[k]s_{im}[n-1-k]\right) \\
\hline
0 \\
\hline
0
\end{array}\right] \tag{25}
$$

From (31) the equations for the coefficients of the terms of the same order can be obtained:

$$
\begin{aligned}
&2(n+1)H_{im}s_{im}[n+1] = \\
&r_{0im}\left(T_{0im}\delta_{n,0} + T_{1im}s_{im}[n] + T_{2im}\sum_{i+j=n} s_{im}[i]s_{im}[j]\right) + \\
&r_{1im}\left(T_{0im}\delta_{n,1} + T_{1im}s_{im}[n-1] + T_{2im}\sum_{i+j=n} s_{im}[i]s_{im}[j]\right) - \\
&\Re\left\{\sum_{i+j=n} V_{Mim}[i]I^*_{Rim}[j]\right\}.
\end{aligned} \tag{34}
$$

It shows that $s_{im}[n]$ can be derived from all the terms of orders up to $n-1$. The equations of induction motors in HE-III are similar to (25). Remove the third equation of (25), substitute $s_{im}[n]$ into other equations (25), and eliminate $I_{Rim\mathrm{Re}}[n]$, $I_{Rim\mathrm{Im}}[n]$ terms will get similar relationship between $I_{Lim\mathrm{Re}}[n]$, $I_{Lim\mathrm{Im}}[n]$ and $C_i[n]$, $D_i[n]$ like (29), and then the following procedure is the same with HE-II.

HE-III flexibly allows dynamic modeling on only part of the motors while maintaining steady-state modeling on the other motors. The motors modeled in steady-state have the same formulation as that in HE-II.

III. VSA USING HOLOMORPHIC EMBEDDING

A. Extend effective range by using Padé approximation

A power series usually has a limited radius of convergence, so the series derived by HE become ineffective beyond the radius. Moreover, the truncated power series tends to have an even smaller effective range under given accuracy tolerance. To overcome such a disadvantage of power series, the Padé approximants can be used to extend the effective range [12], [13]. Although some extra computation is needed for deriving the Padé approximants from power series, the HE using Padé approximants still has advantage in VSA because of its much better convergence than power series. So in this paper, the Padé approximants are used for the approximation of solutions.

B. Multi-stage HE scheme [19]

Even with Padé approximants, the effective range of approximation is still limited. Increasing the terms of Padé approximants can help extend the effective range. But when the number of terms reaches a certain level, increasing it has little effect in extending the effective approximation range. Also, adding terms costs more time in deriving Padé approximants. In this paper, the number of Padé approximants terms is limited by N_P, and in VSA, the effectiveness of approximants is checked by comparing the equation balance with a tolerance ε_E. The furthest point on the system state trace satisfying the equation imbalance below ε_E is designated as the starting point of the next stage. Such a multi-stage scheme guarantees the accuracy of simulation until the collapse point without requiring too many Padé terms, which saves computation time.

A remark is worth noticing on the modeling of the mechanical torque of induction motors. In this paper the mechanical torque adopts the commonly-used quadratic form (11), but HE can also handle more general mechanical torque models. For example, $T_{im}(s_{im})$ as even higher-order polynomials can also be solved with HE. Although the equations need modification, the methodology is the same. Even more generally, $T_{im}(s_{im})$ in other forms can also be solved with HE. If $T_{im}(s_{im})$ is not in a polynomial form, then it can be approximated with Taylor expansion as a truncated polynomial $T'_{im}(s_{im})$. In this case, the initial state s_{im0} can be selected as the original point of Taylor expansion, and since this involves approximation, the error can be tracked and controlled by using the multi-stage HE scheme. Also, the switching of segments can also be achieved with the multi-stage HE scheme.

C. Partial-QSS voltage stability analysis scheme [10]

The procedure for VSA using the partial-QSS method [10] is shown in Fig. 2. We assume the ZIP/motor load grows continuously at a certain pattern with time. Here we name the method as "partial-QSS" because the simulation starts with standard QSS method, but some motors switch to dynamic model during the simulation. The multi-stage HE is used in simulation, and when singularity occurs, the type of singularity

is examined by using participation factors [10]. First, the Jacobian matrix $\mathbf{J}$ of all the algebraic equations (including the power flow equations on all buses and the equilibrium equations of rotor motion of motors that are under QSS assumption) is derived, then apply eigen decomposition to $\mathbf{J}$:

$$\mathbf{J} = \mathbf{P}\mathbf{\Lambda}\mathbf{Q}, \tag{35}$$

and select the left and right eigenvectors $\mathbf{p}_i$ and $\mathbf{q}_i$ corresponding to the smallest eigenvalue λ_i. Then the participation factors of the jth algebraic equation are:

$$\pi_j = p_{ij}q_{ij}. \tag{36}$$

If any motor corresponds to a participation factor much larger than the others (e.g. over 10 times that of any other), then identify local singularity caused by the motor, switch the motor to dynamic model in HE-III, and continue simulation. Otherwise, if the participation factor of all motors are very small, then the singularity is likely to be global.

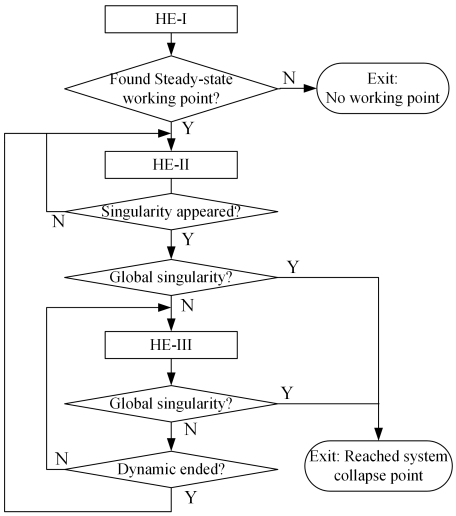

Fig. 2. Flowchart of partial-QSS VSA.

D. Full-dynamic simulation

With HE-III, the time-domain simulation with dynamic modeling of all motors can be implemented. The simulation starts from a steady-state starting point derived by HE-I, and then the multi-stage HE-III simulates system dynamics until meeting global singularity. The full-dynamic simulation with HE-III should be more accurate than the partial-QSS method, and a significant boost in computation speed is expected as compared with traditional numerical integration method.

IV. Test cases

A. IEEE 14-bus system

IEEE 14-bus system has 11 PQ buses, 4 PV buses and 1 slack bus. To test the HE in VSA with induction motors, the IEEE 14-bus system is modified so that each PQ bus is connected with an induction motor load. The average percentage of induction motor load is 42.2%.

First test the HE-I in solving power flow. In HE, different numbers of Padé approximant terms N_P are selected, and the results are checked with the maximum absolute imbalance of the equations. As shown in Table. I, as N_P grows, the maximum equation imbalance decreases significantly, but the computation time increases. The N_P can be chosen based on the actual demand of accuracy and computation speed.

TABLE I
Accuracy and efficiency of HE-I in IEEE 14-bus system case

N_P	Max. equation imbalance (pu)	Computation time (s)
5	9.6×10^{-3}	0.019
10	1.4×10^{-3}	0.030
15	4.9×10^{-5}	0.043
20	3.0×10^{-7}	0.058
30	6.3×10^{-10}	0.074
40	1.7×10^{-11}	0.091

Next study the system state evolution under load increase. The mechanical torque of induction motors is assumed as $T_{im} = T_0(1 - s_{im}^2)$. In the 14-bus system, increase the PQ load by 10% of base state value per second, and increase the mechanical load by 2% per second, then use HE-II and HE-III to do steady-state and dynamic simulations, respectively. For both HE-II and HE-III, $N_P = 20$. Under QSS assumptions, the simulation stops at $t = 6.286$s, as Fig. 3 shows, the imbalance of equations under HE-II is below 10^{-5}, showing that the HE-II itself is accurate. As Fig. 4 shows, the steady-state solution exists at the intersection of the electric torque and mechanical torque curves. At practical working points, the slip is close to 0 (the left intersection point in Fig. 4). When mechanical load increases (mechanical torque rises) or voltage decreases (electric torque drops), the intersection point will move towards the peak point of the electric torque with slip increase. As mechanical load increases or voltage drops to some extent, the intersection point near $s_{im} = 0$ disappears, which is a bifurcation, and the motor starts to stall. The state of a stalling motor then moves to the only steady-state solution near $s_{im} = 1$. As Fig. 5 shows, the termination point of simulation approximately matches the maximum electric torque point of motor 4, which verifies the local bifurcation caused by the motor [10]. At the local bifurcation point, there is no steady-state solution in the vicinity, but it does not mean the collapse of the whole system. The system can still operate with increasing load, but the stalling motor should be simulated in dynamic model (as was treated in [10]), or alternatively, all the motors can be simulated with dynamic models from the very beginning. We use HE-III to simulate the dynamics of all the induction motor loads, and as Fig. 5 shows, the HE-III successfully simulates the stalling of the motor. Fig. 6 compares the results of HE-III with that of the modified Euler method (a commonly-used numerical integration method), it shows that the difference of bus voltages is below 10^{-4} for the entire time span, and for 99% of the time span, the difference is below 10^{-6}.

The results of HE is compared with those of the modified Euler method under different time steps. For the modified Euler method, time steps of $\Delta t = 0.01$s, $\Delta t = 0.005$s and

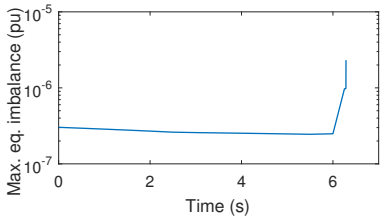

Fig. 3. Imbalance of power flow equations of HE-II.

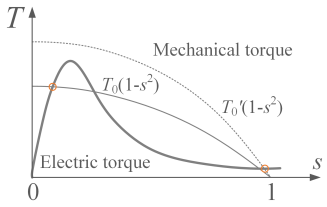

Fig. 4. Illustration of induction motor steady-state solutions (denoted by the circles at the intersections of the curves).

$\Delta t = 0.002$s are selected. The metric selected for comparison is the maximum imbalance of the DAEs. The results are shown in Fig. 7. It can be seen that the equation imbalance of the modified Euler method is much higher than that of HE-III. Although reducing the time step achieves lower imbalance, to achieve the same level of accuracy as HE-III, the time step of the modified Euler method needs to be around $\Delta t = 10^{-4}$s, which is impractically small. Therefore, HE-III has significant advantage in accuracy over the modified Euler method as a traditional numerical integration method.

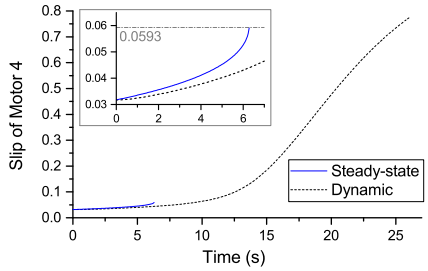

Fig. 5. Slip of motor on bus 4 in IEEE 14-bus system. The horizontal line in the small figure corresponds to the slip at the maximum electric torque.

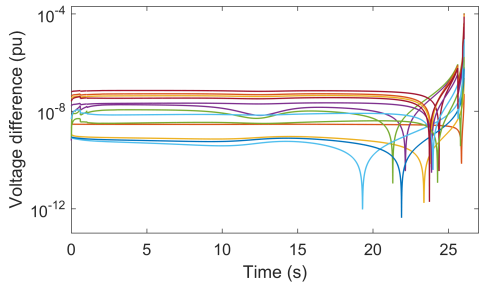

Fig. 6. Difference of voltage between HE-III and the modified Euler methods.

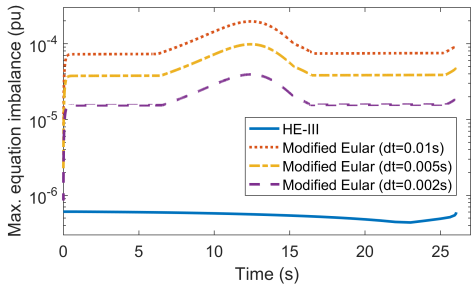

Fig. 7. Imbalance of equations: HE-III and the modified Euler methods.

B. NPCC 140-bus system

The NPCC system model [24] has 140 buses, including 45 PV buses, 94 PQ buses and 1 slack bus. The system is also modified to add 54 induction motors to 54 PQ buses. Moreover, ZIP loads can also be added to these buses. To demonstrate the performance of the proposed method and compare different load models, three system models are provided for analysis: 1) PQ modeling of load only, 2) ZIP modeling of load, and 3) ZIP and induction motors.

The parameters of the ZIP and motor loads are adjusted so that under the base condition, the system state is the same as the original PQ-load only system model. The percentage of each type of load on the 54 buses are shown in Fig. 8. For the system model with ZIP load, the average percentage of the ZIP components are: 17.0% for "Z", 17.9% for "I" and 65.1% for "P". And for system model with ZIP and induction motor load, the average load components are: 8.0% for "Z", 6.4% for "I", 51.5% for "P", and 34.1% for motor.

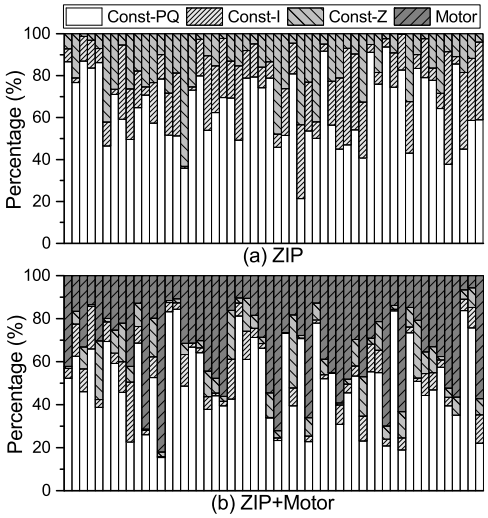

Fig. 8. Percentage by load type on 54 load buses in NPCC system. (a) ZIP load model; (b) ZIP + Motor load model. The x-axis represents the load buses.

The system models with only PQ loads or ZIP loads do not have dynamic models, so the long-term VSA can be studied with multi-stage HE-II. Assume the load increase on each bus is 5% of its base state value per second. The time consumption and the number of HE stages are listed in Table. II. For comparison, the continuation power flow (CPF) in PQ-load

model case takes 57 steps and 2.69s at best performance. This test verifies satisfactory efficiency of the proposed HE method.

TABLE II
PERFORMANCE OF HE IN STATIC VSA

Load model	Stages	Time (s)
PQ	4	0.65
ZIP	7	1.41

Next test the dynamic simulation with induction motor loads. In the NPCC system model, the inertial constants of induction motors H_{im} range from 0.5s-2s, and the average value is 1.22s. The mechanical loads of induction motors increase by 10% of base case values per second, and the other types of loads increase by 5% of the base case value per second. First use the partial-QSS method [10] implemented in HE for simulation, and the motor slips are shown in Fig. 9. Results show that the collapse point simulated by partial-QSS scheme is at 7.856s.

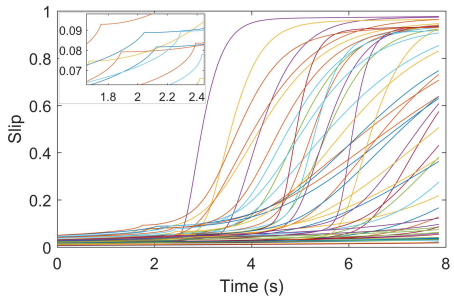

Fig. 9. Motor slips of NPCC system obtained by partial-QSS with HE (ZIP+Motor loads). The small figure shows the switching points when induction motors start to stall.

Full-dynamic simulation with HE-III is also conducted in the same system. The voltage of buses and motor slips are shown in Figs. 10 and 11. With full-dynamic simulation, the system collapse point is reached at 7.856s. The system state traces are also benchmarked with traditional numerical integration methods, and the differences of bus voltages are shown in Fig. 12. The result shows that the voltage difference is under 2×10^{-4}p.u. for over 99% of the time span, and the difference is under 1.5×10^{-3}p.u. for the entire process, which shows satisfactory accuracy of the proposed HE method.

In this case, the partial-QSS simulation results are also quite close to those derived by full-dynamic simulation. But due to QSS assumption, the accuracy is compromised. Also, the HE using the partial-QSS scheme is not as efficient as full-dynamic HE. The partial-QSS scheme needs additional efforts for switching motors from static to dynamic model. Moreover, the switching of motor models causes errors with the equations, and thus shortens the length of each stage that HE can reach. Fig. 13 shows that the equation imbalance of partial-QSS scheme grows significantly where many motors switch to dynamic model, and finally causing more than 10 times the equation imbalance that of full-dynamic simulation scheme. In contrast, the full-dynamic simulation scheme implemented in HE has nearly stable equation imbalance.

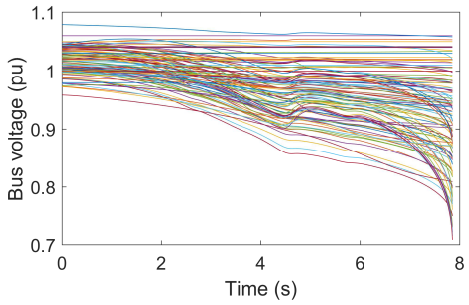

Fig. 10. Bus voltage of NPCC system (ZIP+Motor load).

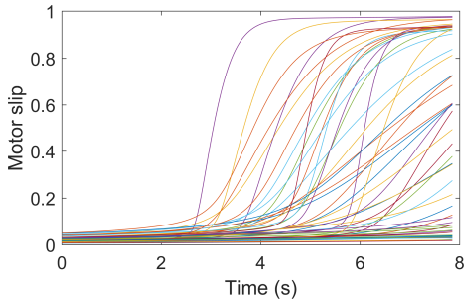

Fig. 11. Motor slip in NPCC system (ZIP+Motor load).

In terms of computation efficiency, Table. III compares the modified Euler method, the HE with partial-QSS scheme, and HE full-dynamic simulation. The modified Euler method uses a fixed step length of 0.002s, which is the largest available step length without causing a significant numerical simulation error. The partial-QSS simulation implemented with HE is much faster than the numerical integration method. Nevertheless, the full-dynamic simulation with HE is even faster, and it is also advantageous in accuracy. These test results exhibit the promising potential of holomorphic embedding in dynamic analysis of power systems.

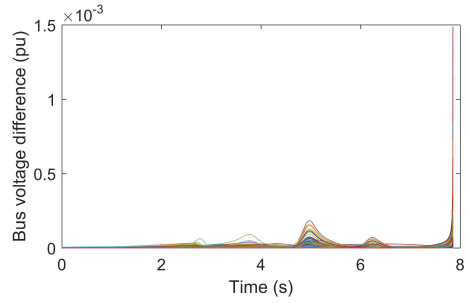

Fig. 12. Comparison between HE (full-dynamic) and modified Euler method.

TABLE III
COMPUTATIONAL EFFICIENCY COMPARISON IN NPCC SYSTEM

Simulation methods	Stages/Steps	Avg. step len.(s)	Time cost(s)
Modified Euler	3928	0.002	1150.1
HE (partial-QSS)	105	0.0748	31.19
HE (full-dynamic)	55	0.143	13.95

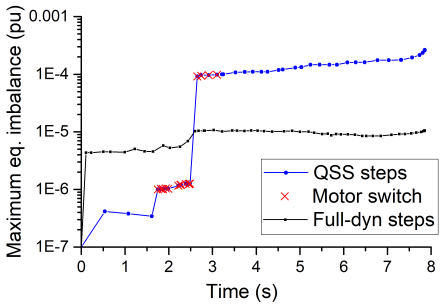

Fig. 13. Comparison of steps and equation mismatch between partial-QSS and full-dynamic schemes.

C. Polish test system

To further demonstrate the capability of the proposed approach for VSA, Polish test system [25] is utilized in this case. The system has 2383 buses, including 2056 PQ buses and 326 PV buses. There are 1562 ZIP loads and 1542 induction motors in the system. In such a complex test, the Newton-Ralphson method faces difficulty in solving the nonlinear algebraic equations of the system, so for the traditional numerical integration approaches, the time step is restricted to a very small value. By testing, the time step for the modified Euler method is set as 0.002s. Assume the PQ/ZIP load increase on each bus is 10% of its base-state value per second, and the mechanical torque of each induction motor increases by 50% of its base-state value per second. The results of the two methods match well. As Fig. 14 shows, the difference of bus voltage is below 2×10^{-4}p.u. for above 99% of the time span. But in terms of computational efficiency, the two approaches differ significantly. The HE is significantly faster than the modified Euler method. And the result shows that the VSA based on HE can be finished within a minute on the Polish system with many static and dynamic loads, so this HE-based approach is promising for accurate online VSA.

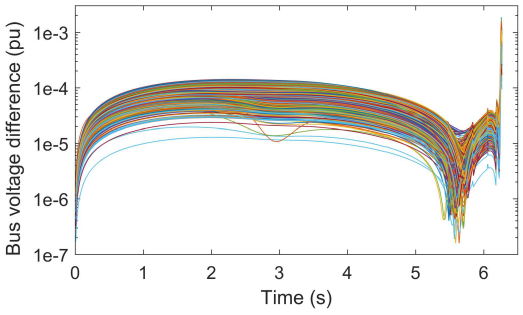

Fig. 14. Comparison of results between HE (full-dynamic) and modified Euler method on Polish test system.

V. Conclusion

This paper proposes a set of systematic solutions for voltage stability analysis (VSA) with induction motor loads by using holomorphic embedding (HE). Three formulations of HE are proposed for solving power system, QSS state trace under load increase, and system dynamics under load increase, respectively. The algorithms for solving the three HE formulations are also elucidated. Then, with Padé approximation and multi-stage continuation techniques to extend the effective range of HE, the partial-QSS simulation and full-dynamic simulation methods based on HE are realized, respectively. This paper is the first research work which applies HE in dynamic simulation for VSA of power systems.

TABLE IV
Computational efficiency comparison in Polish system

Simulation methods	Time cost(s)
Modified Euler	2840.4
HE (full-dynamic)	28.63

The proposed VSA methods based on HE are tested on the IEEE 14-bus test system, an NPCC 140-bus system and Polish 2383-bus system. By comparing with traditional methods such as continuation power flow and dynamic simulation based on numerical integration, the accuracy of the proposed HE-based methods is verified. Moreover, the tests on NPCC 140-bus system and Polish 2383-bus system shows that the proposed HE method is significantly faster than that of the modified Euler method, which reveals very promising potential of holomorphic embedding methodology in dynamic analysis of power systems.

Appendix A
The convergence of HE-I

The HE-I formulation (10) is equivalent to an induction motor with excitation impedance as Z_{eim}/α, and mechanical torque characteristics as $\alpha T_{im}(s_{im})$. The desired solution is at $\alpha = 1$. Without losing generality, assume the external voltage V_i to be constant. Eliminating V_{Mim}, I_{Rim} and I_{Lim}, the equations (10) can be converted to one equation denoted as $g(s_{im}, \alpha) = 0$. Specifically, $g(s_{im}, \alpha) = 0$ represents the balance between electric torque T_{ie} and mechanical torque T_{im}, which can be further written as $T_{ie}(s_{im}, \alpha) - \alpha T_{im}(s_{im}) = 0$. For $g(s_{im}, \alpha) = 0$ we have the following remark:

Remark A1: According to the implicit function theorem (ImFT) [26], at a point (s_{im0}, α_0) satisfying $g(s_{im0}, \alpha_0) = 0$, if $\frac{\partial g}{\partial s_{im}}$ is invertible, then there exists an open interval U containing α_0, and in U exists a unique continuous differential function $s_{im}(\alpha)$ satisfying $g(s_{im}(\alpha), \alpha) = 0$ for all $\alpha \in U$. Additionally, as $g(s_{im}, \alpha)$ is analytic (i.e. infinitely differentiable), $s_{im}(\alpha)$ is also an analytic function where $\alpha \in U$, which means the Taylor series of $s_{im}(\alpha)$ about $\forall \alpha_0' \in U$ converges to the function $s_{im}(\alpha)$ in a domain $U_R \subset U$.

Noticing that Z_{eim}/α usually has a large value, ignoring the excitation branch on the equivalent circuit does not incur much error, but the equation is much simpler:

$$\frac{|V_i|^2 R_{2im} s_{im}}{R_{2im}^2 + 2R_{2im}R_{1im}s_{im} + [R_{1im}^2 + (X_{1im} + X_{2im})^2]s_{im}^2} - \alpha T_{im}(s_{im}) = 0 \quad (37)$$

The first term as approximately the electric torque of the induction motor does not change with α, and the second term

is α times the mechanical torque characteristics. The solution s_{im} is the intersection point of electric torque and mechanical torque, as is shown in Fig. 15. From $\alpha = 0$, $s_{im} = 0$, as α grows from 0 to 1, according to the *Remark A1*, $s_{im}(\alpha)$ is continuous if $\frac{\partial g}{\partial s_{im}} \neq 0$. And since $s_{im}(\alpha)$ is analytic, in a neighborhood of a given α_0, $s_{im}(\alpha)$ can always be approximated by the Taylor series about α_0. Therefore, on the condition that $\frac{\partial g}{\partial s_{im}} \neq 0$ in $\alpha \in [0, 1]$, the solution of (10) can be satisfactorily approximated by using multi-stage HE.

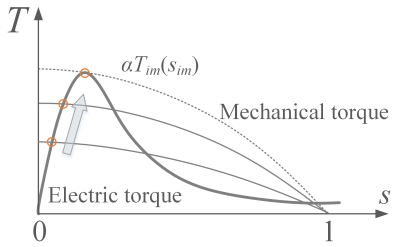

Fig. 15. Illustration of the steady-state slip of an induction motor.

Noticing that $g(s_{im}, \alpha) = T_{ie}(s_{im}, \alpha) - \alpha T_{im}(s_{im})$, the condition $\frac{\partial g}{\partial s_{im}} \neq 0$ is equivalent to $\frac{\partial T_{ie}(s_{im},\alpha)}{\partial s_{im}} \neq \frac{\partial \alpha T_{im}(s_{im})}{\partial s_{im}}$. For an induction motor, a stable operating point must satisfy $\frac{\partial T_{ie}(s_{im},\alpha)}{\partial s_{im}} > \frac{\partial \alpha T_{im}(s_{im})}{\partial s_{im}}$. So the low-slip stable operating points satisfy $\frac{\partial g}{\partial s_{im}} \neq 0$ in $\alpha \in [0, 1]$, and thus the HE solution starting from $s_{im} = 0$ converges to the low-slip solution.

REFERENCES

[1] L. Pereira, D. Kosterev, P. Mackin, D. Davies, J. Undrill, and W. Zhu, "An interim dynamic induction motor model for stability studies in the wscc," *IEEE Trans. Power Syst*, vol. 17, no. 4, pp. 1108–1115, 2002.

[2] D. Kosterev *et al.*, "Load modeling in power system studies: Wecc progress update," in *IEEE PES General Meeting*, 2008, pp. 1–8.

[3] W. W. Price *et al.*, "Load modeling for power flow and transient stability computer studies," *IEEE Trans. Power Syst*, vol. 3, no. 1, pp. 180–187, 1988.

[4] Y. Sekine and H. Ohtsuki, "Cascaded voltage collapse," *IEEE Trans. Power Syst*, vol. 5, no. 1, pp. 250–256, 1990.

[5] R. Balanathan *et al.*, "Modelling induction motor loads for voltage stability analysis," *International journal of electrical power & energy systems*, vol. 24, no. 6, pp. 469–480, 2002.

[6] T. Van Cutsem and C. D. Vournas, "Voltage stability analysis in transient and mid-term time scales," *IEEE Trans. Power Syst*, vol. 11, no. 1, pp. 146–154, 1996.

[7] D. J. Hill, "Nonlinear dynamic load models with recovery for voltage stability studies," *IEEE Trans. Power Syst*, vol. 8, no. 1, pp. 166–176, 1993.

[8] B. Wang, B. Fang, Y. Wang, H. Liu, and Y. Liu, "Power system transient stability assessment based on big data and the core vector machine," *IEEE Trans. Smart Grid*, vol. 7, no. 5, pp. 2561–2570, 2016.

[9] H. Pulgar-Painemal, Y. Wang, and H. Silva-Saravia, "On inertia distribution, inter-area oscillations and location of electronically-interfaced resources," *IEEE Trans. Power Syst*, vol. 33, no. 1, pp. 995–1003, 2018.

[10] C. Vournas *et al.*, "Modelling of stalling motors during voltage stability studies," *IEEE Trans. Power Syst*, vol. 13, no. 3, pp. 775–781, 1998.

[11] A. Trias, "The holomorphic embedding load flow method," in *IEEE PES General Meeting*, 2012, pp. 1–8.

[12] H.-D. Chiang, T. Wang, and H. Sheng, "A novel fast and flexible holomorphic embedding method for power flow problems," *IEEE Trans. Power Syst*, 2017.

[13] S. Rao, Y. Feng, D. J. Tylavsky, and M. K. Subramanian, "The holomorphic embedding method applied to the power-flow problem," *IEEE Trans. Power Syst*, vol. 31, no. 5, pp. 3816–3828, 2016.

[14] C. Liu, B. Wang, F. Hu, K. Sun, and C. L. Bak, "Online voltage stability assessment for load areas based on the holomorphic embedding method," *IEEE Trans. Power Syst*, vol. 33, no. 4, pp. 3720–3734, 2018.

[15] A. Trias and J. L. Marín, "The holomorphic embedding loadflow method for dc power systems and nonlinear dc circuits," *IEEE Trans. Circuits Syst I Regul Pap*, vol. 63, no. 2, pp. 322–333, 2016.

[16] M. Basiri-Kejani and E. Gholipour, "Holomorphic embedding load-flow modeling of thyristor-based facts controllers," *IEEE Trans. Power Syst*, vol. 32, no. 6, pp. 4871–4879, 2017.

[17] S. D. Rao, D. J. Tylavsky, and Y. Feng, "Estimating the saddle-node bifurcation point of static power systems using the holomorphic embedding method," *International Journal of Electrical Power & Energy Systems*, vol. 84, pp. 1–12, 2017.

[18] C. Liu, B. Wang, X. Xu, K. Sun, D. Shi, and C. L. Bak, "A multi-dimensional holomorphic embedding method to solve ac power flows," *IEEE Access*, vol. 5, pp. 25 270–25 285, 2017.

[19] B. Wang, C. Liu, and K. Sun, "Multi-stage holomorphic embedding method for calculating the power-voltage curve," *IEEE Trans. Power Syst*, vol. 33, no. 1, pp. 1127–1129, 2018.

[20] F. Milano, *Power system modelling and scripting*. Springer Science & Business Media, 2010.

[21] R. Yao, F. Liu, G. He, B. Fang, and L. Huang, "Static security region calculation with improved cpf considering generation regulation," in *IEEE International Conference on Power System Technology (POWERCON)*, 2012, pp. 1–6.

[22] R. Yao, S. Huang, K. Sun, F. Liu, X. Zhang, and S. Mei, "A multi-timescale quasi-dynamic model for simulation of cascading outages," *IEEE Trans. Power Syst*, vol. 31, no. 4, pp. 3189–3201, 2016.

[23] R. Yao, K. Sun, F. Liu, and S. Mei, "Management of cascading outage risk based on risk gradient and markovian tree search," *IEEE Trans. Power Syst*, vol. 33, no. 4, pp. 4050–4060, 2018.

[24] J. H. Chow and K. W. Cheung, "A toolbox for power system dynamics and control engineering education and research," *IEEE Trans. Power Syst*, vol. 7, no. 4, pp. 1559–1564, 1992.

[25] R. D. Zimmerman *et al.*, "Matpower: Steady-state operations, planning, and analysis tools for power systems research and education," *IEEE Trans. Power Syst*, vol. 26, no. 1, pp. 12–19, 2011.

[26] S. G. Krantz and H. R. Parks, *The implicit function theorem: history, theory, and applications*. Springer Science & Business Media, 2012.

Rui Yao (S'12–M'17) received the B.S. degree (with distinction) in 2011 and Ph.D. degree in 2016 in electrical engineering at Tsinghua University, Beijing, China. He was a postdoctoral research associate at the University of Tennessee, Knoxville during 2016–2018. He is currently a postdoctoral appointee at Argonne National Laboratory.

Kai Sun (M'06–SM'13) received the B.S. degree in automation in 1999 and the Ph.D. degree in control science and engineering in 2004 from Tsinghua University, Beijing, China. He is currently an associate professor at the Department of EECS, University of Tennessee, Knoxville.

Di Shi (M'12–SM'17) received the B. S. degree in electrical engineering from Xian Jiaotong University, Xian, China, in 2007, and M.S. and Ph.D. degrees in electrical engineering from Arizona State University, Tempe, AZ, USA, in 2009 and 2012, respectively. He currently leads the PMU & System Analytics Group at GEIRI North America, San Jose, CA, USA. His research interests include WAMS, Energy storage systems, and renewable integration. He is an Editor of IEEE Transactions on Smart Grid.

Xiaohu Zhang (S'12–M'17) received the B.S. degree in electrical engineering from Huazhong University of Science and Technology, Wuhan, China, in 2009, the M.S. degree in electrical engineering from Royal Institute of Technology, Stockholm, Sweden, in 2011, and the Ph.D. degree in electrical engineering at The University of Tennessee, Knoxville, in 2017. Currently, he works as a power system engineer at GEIRI North America, San Jose, CA.